

Article

# Assembly of a G-Quadruplex Repair Complex by the FANCI DNA Helicase and the REV1 Polymerase

Kaitlin Lowran <sup>1</sup>, Laura Campbell <sup>1</sup>, Phillip Popp <sup>2</sup> and Colin G. Wu <sup>1,\*</sup> 

<sup>1</sup> Department of Chemistry, Oakland University, Rochester, MI 48309, USA; kalowran@oakland.edu (K.L.); lcampbell2@oakland.edu (L.C.)

<sup>2</sup> Case Western Reserve University, Cleveland, OH 44106, USA; ppp19@case.edu

\* Correspondence: colinwu@oakland.edu; Tel.: +1-248-370-2349

Received: 29 November 2019; Accepted: 17 December 2019; Published: 19 December 2019



**Abstract:** The FANCI helicase unfolds G-quadruplexes (G4s) in human cells to support DNA replication. This action is coupled to the recruitment of REV1 polymerase to synthesize DNA across from a guanine template. The precise mechanisms of these reactions remain unclear. While FANCI binds to G4s with an AKKQ motif, it is not known whether this site recognizes damaged G4 structures. FANCI also has a PIP-like (PCNA Interacting Protein) region that may recruit REV1 to G4s either directly or through interactions mediated by PCNA protein. In this work, we measured the affinities of a FANCI AKKQ peptide for G4s formed by (TTAGGG)<sub>4</sub> and (GGGT)<sub>4</sub> using fluorescence spectroscopy and biolayer interferometry (BLI). The effects of 8-oxoguanine (8oxoG) on these interactions were tested at different positions. BLI assays were then performed with a FANCI PIP to examine its recruitment of REV1 and PCNA. FANCI AKKQ bound tightly to a TTA loop and was sequestered away from the 8oxoG. Reducing the loop length between guanine tetrads increased the affinity of the peptide for 8oxoG4s. FANCI PIP targeted both REV1 and PCNA but favored interactions with the REV1 polymerase. The impact of these results on the remodeling of damaged G4 DNA is discussed herein.

**Keywords:** G-quadruplexes (G4s); 8-oxoguanine (8oxoG); helicases; FANCI; REV1; PCNA; DNA repair; fluorescence spectroscopy; biolayer interferometry; circular dichroism

## 1. Introduction

### 1.1. What are G-Quadruplexes?

G-quadruplexes (or G4s) are stable secondary structures formed by guanine-rich nucleic acids. Single-stranded (ss) DNA sequences possessing four runs of three or more successive guanine bases can fold into G4s by Hoogsteen hydrogen bonding [1]. Their interactions are further stabilized by potassium or sodium cations. Depending on solution conditions and the intervening loop sequences, G4s can adopt parallel, antiparallel, or hybrid conformations [2,3]. These spatial arrangements have distinct optical properties that can be distinguished by circular dichroism (CD) spectroscopy [4]. Due to their inherent stability, the accumulation of G4s is toxic to cells, as it disrupts essential biological processes such as DNA replication and repair, RNA transcription, as well as mRNA translation [5]. However, by regulating where and when G4s can form, their presence can provide additional means to control gene expression and protein synthesis [6,7]. G4s are therefore attractive therapeutic targets for genetic diseases including cancer, heart failure, and Fanconi anemia [8–14]. Recent studies have shown that G4s are ubiquitous throughout the human genome with over 400,000 unique G4-forming DNA sequences [15,16]. A growing number of helicases and polymerases have emerged as key enzymes

that unfold G4s in human cells [17–24]. Their activities are needed at G4s in a timely manner not only to maintain genetic stability, but also support cellular functions.

### 1.2. How Are G4s Removed in Cells?

Helicases and polymerases are motor proteins that couple the chemical energy from nucleotide binding and hydrolysis to do mechanical work [25–27]. Energy is consumed to facilitate translocation along nucleic acids and the removal of secondary structures within the lattice. Helicases are best known for their unwinding activity, which separates double-stranded (ds) DNA or dsRNA to form transient single-stranded (ss) intermediates [28,29]. Although polymerases function mainly in nucleic acid synthesis, some can unwind short duplexes with their binding free energy alone [30,31]. Similarly, the RecBCD and NS3 helicases can melt out several base pairs upon interacting with their targets in the absence of ATP [32,33]. Because helicases and polymerases are potent remodelers of nucleic acids, most enzymes exhibit robust G4-binding and/or unfolding activity *in vitro* [1]. Several have also been shown to act on G4s *in vivo* based on genetic and cell-based evidence. These include the XPD-family FANCI and RTEL1 helicases [17,20], the RecQ-family WRN and BLM helicases [34,35], the Pif1 helicase [36], the REV1 DNA repair polymerase [37], and others reviewed here [1,38]. Defects in these enzymes stall replication and repair at G4 DNA. The molecular basis by which they are recruited to G4s are becoming clearer. REV1 has a high affinity for G4-containing sequences [18]. RecQ helicases have a conserved domain that binds directly to G4s [39]. The RHAU (or DHX36) helicase recognizes G4 RNA through a special motif at the protein N-terminus [40]. In solution, this site adopts an  $\alpha$ -helix that is followed by an AKKQ loop [41]. It is thought that the helix stacks on top of a guanine tetrad while lysine residues within the AKKQ are anchored into the RNA backbone. FANCI possesses an AKKQ motif that is flanked by a comparable G4-targeting peptide [42]. Enzymes participating in G4-maintenance have developed strategies to detect G4s in cells; their motor activities then take over to unfold these structures. One question remains a major barrier to research progress—how are damaged G4s processed within the cell? While the same helicases and polymerases may be involved, the presence of damage within a G4 presents an additional challenge for the enzymes to overcome. Guanine bases are vulnerable to reactive oxygen species that can convert them into 8-oxoguanines (8oxoGs). 8oxoG-modified G4s (8oxoG4s) can still fold into stable structures [43,44]. This work will use FANCI as a model system to examine the molecular recognition of damaged G4 DNA.

### 1.3. What Is the Role of FANCI in G4 Repair?

The FANCI helicase participates in the repair of interstrand crosslinks in human cells. Mutations in FANCI or related proteins of this pathway can lead to Fanconi anemia, a rare disease marked by progressive bone marrow failure and increased susceptibility to cancer [45–48]. At least 23 Fanconi anemia complementation (FANC) groups have been identified that function in the initial binding of the lesion, incision of the two DNA strands, or resolution of the newly generated dsDNA break [48]. Not surprisingly, many FANC proteins are components of the nucleotide excision repair and homologous recombination machinery. FANCI coordinates the repair of DNA intermediates that arise from these reactions [42,49,50]. It unfolds G4s *in vitro* and this activity supports DNA replication through G4-forming regions [12,17]. FANCI binds to G4s with a modular insertion that is not found in other XPD-family members [42]. The unrelated RHAU RNA helicase shares this G4-binding site, but it is not known if FANCI can function at 8oxoG4s [40,41]. In a current model, FANCI repeatedly unfolds and refolds G4s near a stalled replication fork to keep the strand clear for a repair polymerase [42]. The REV1 translesion DNA synthesis polymerase has been suggested for this role because it prefers to incorporate cytosine across from any templated base [51]. REV1 also has a higher affinity for G4-containing DNA and disrupts its structure upon loading [18]. Repair polymerases are commonly recruited to damaged DNA via interactions with the PCNA sliding clamp [52]. Their contacts are mediated through a PCNA Interacting Peptide (or PIP) motif [53]. PIP-boxes have loosely defined consensus residues. Diverging PIP-like sequences can bind to other repair proteins including REV1 [54–56]. Because FANCI has

a potential PIP-motif based on its primary amino acid sequence, we hypothesize that this site can function either as a canonical PIP that recruits REV1 through interactions with PCNA, or as an REV1 Interacting Region (RIR) that brings the polymerase directly to G4s [42,54,55]. To test this, we have developed a biolayer interferometry assay (BLI) to monitor the molecular interactions between the FANCI PIP, REV1, and PCNA. We have also validated this approach using fluorescence spectroscopy to probe the binding of FANCI AKKQ to 8oxoG4s.

## 2. Materials and Methods

### 2.1. Buffers and Reagents

All buffers and reagents were prepared with reagent-grade chemicals and double distilled water that was further purified with a Smart2Pure 6 UV/UF system (ThermoFisher, Waltham, MA, USA). Solutions were sterilized through a 0.22 micron PES filter. Experiments were performed at 25 °C in Buffer H (20 mM HEPES pH 7.5, 150 mM KCl, 5 mM TCEP, and 5% (v/v) glycerol) unless otherwise specified.

### 2.2. FANCI Peptides and DNA Oligos

FANCI peptides were synthesized by Genscript (Piscataway, NJ, USA). Lyophilized powders were dissolved in Buffer H, and peptide concentrations were determined using a NanoDrop One UV-Vis microvolume spectrophotometer (ThermoFisher) and the molar extinction coefficients ( $\epsilon_{280}$ ) below (Table 1). Oligodeoxyribonucleotides were purchased from Integrated DNA Technologies (IDT, Coralville, IA, USA). DNA oligos were prepared similarly in Buffer H, and their stock concentrations were determined spectrophotometrically with the following molar extinction coefficients ( $\epsilon_{260}$ ). Peptide samples were aliquoted, frozen, and stored at -20 °C until use. DNA substrates were stored at 4 °C. Prior to use, G4 substrates were heated to 95 °C for ten minutes followed by cooling to 25 °C over two hours to promote G4-formation.

**Table 1.** Peptide sequences and DNA sequences.

Peptide Sequences			
Name	Sequence (N→C)	Molar Extinction Coefficient (M <sup>-1</sup> cm <sup>-1</sup> )	Purpose
FANCI AKKQ-W	SPEKTTLAAKLSAKKQASIW	5500	Fluorescence and BLI
bioFANCI PIP	Biotin-SWSSFNSLGQYFTGKIP	6990	BLI
bioFANCI PIP AA	Biotin-SWSSFNSLGQAATGKIP	5500	BLI
DNA Sequences			
Name	Sequence (5'→3')	Molar Extinction Coefficient (M <sup>-1</sup> cm <sup>-1</sup> )	Purpose
(TTAGGG) <sub>4</sub>	TTAGGGTTAGGGTTAGGGTTAGGG	244,600	Fluorescence and CD
(TTAGGG) <sub>4</sub> 8oxo1	TTA/i8oxodG/GGTTAGGGTTAGGGTTAGGG	239,000	Fluorescence and CD
(TTAGGG) <sub>4</sub> 8oxo5	TTAGGGTTAG/i8oxodG/GTTAGGGTTAGGG	239,000	Fluorescence and CD
(GGGT) <sub>4</sub>	GGGTGGGTGGGTGGGT	157,200	Fluorescence and CD
(GGGT) <sub>4</sub> 8oxo1	T/i8oxodG/GGTGGGTGGGTGGGT	159,100	Fluorescence and CD
(GGGT) <sub>4</sub> 8oxo5	GGGTG/i8oxodG/GTGGGTGGGT	151,600	Fluorescence and CD
5'bioPEG12-(TTAGGG) <sub>4</sub>	/5Biosg//iSp18//iSp18/TTAGGGTTAGGGTTAGGGTTAGGG	244,600	BLI
5'bioPEG12-(TTAGGG) <sub>4</sub> -8oxo1	/5Biosg//iSp18//iSp18/TTA/i8oxodG/GTTAGGGTTAGGGTTAGGG	239,000	BLI
5'bioPEG12-(TTAGGG) <sub>4</sub> -8oxo5	/5Biosg//iSp18//iSp18/TTAGGGTTAG/i8oxodG/GTTAGGGTTAGGG	239,000	BLI

### 2.3. Recombinant Proteins

The pEB022 plasmid used to produce full-length human PCNA protein was kindly provided by Dr. M. Todd Washington (University of Iowa). A codon-optimized construct (VB170525-1265 nra)

used to express human REV1 CTD (amino acid residues 1157 to 1251) in *E. coli* was synthesized by VectorBuilder Inc. (Chicago, IL, USA). Plasmids were transformed into NiCo21(DE3) competent cells from New England Biolabs (Ipswich, MA, USA). Single bacteria colonies were selected on LB agar plates that were supplemented with 50 µg/mL of kanamycin (PCNA) or carbenicillin (REV1 CTD) to inoculate starter cultures in LB broth. Overnight growths were diluted 1:50 into 4 × 1L LB (37 °C, 250 rpm). Protein expression was induced by adding IPTG to 1 mM when the optical density at 600 nm reached 0.4 absorbance units. Cells were cultured overnight at 16 °C. They were harvested 16 h post induction by centrifugation (6000 × *g* at 4 °C) for 60 min, and the pellets were resuspended in 20 mM NaPi (pH 7.5), 300 mM NaCl, 30 mM imidazole, 1 mM DTT, 5% (*v/v*) glycerol, 1% NP-40, and 1 mM PMSF.

*E. coli* resuspensions were sonicated on ice at 45% amplitude using a Fisher 505 dismembrator (Fisher Scientific, Hampton, NH, USA) equipped with a 12 mm titanium probe. After a sonication time of 15 min (15 s on, 45 s off), lysates were clarified by centrifugation (45,000 × *g* at 4 °C) for 90 min. Supernatant samples were filtered through a 0.22 micron PES membrane prior to liquid chromatography.

All protein purification steps were conducted within a refrigerated cabinet maintained at 4 °C. Filtrates were loaded onto a 20 mL IMAC column (GE Healthcare, Chicago, IL, USA) that was charged with Ni<sup>2+</sup> and equilibrated in 20 mM NaPi (pH 7.5), 300 mM NaCl, 30 mM imidazole, 1 mM DTT, and 5% (*v/v*) glycerol using an AKTA Start FPLC (GE Healthcare). The column was then washed with 200 mL of reduced salt buffer (20 mM NaPi (pH 7.5), 30 mM NaCl, 30 mM imidazole, 1 mM DTT, and 5% (*v/v*) glycerol). PCNA or REV1 CTD was eluted with 20 mM NaPi (pH 7.5), 30 mM NaCl, 1 M imidazole, 1 mM DTT, and 5% (*v/v*) glycerol over a 200 mL linear gradient. Fractions containing PCNA or REV1 CTD were identified by SDS-PAGE, pooled, and loaded onto a 5 mL HiTrap Heparin column (GE Healthcare) that was equilibrated in 20 mM HEPES (pH 7.5), 30 mM NaCl, 5 mM TCEP, and 5% (*v/v*) glycerol using an Azura Bio LC50 FPLC (Knauer, Berlin, Germany). The column was washed with 100 mL of the equilibration buffer to remove trace contaminants. PCNA or REV1 CTD was eluted off the column with 20 mM HEPES (pH 7.5), 1 M NaCl, 5 mM TCEP, and 5% (*v/v*) glycerol over a 50 mL linear gradient. Protein purity was assessed by SDS-PAGE. Samples were dialyzed into Buffer H with 20% (*v/v*) glycerol, aliquoted, and frozen in liquid nitrogen. Purified recombinant proteins were stored at −80 °C until use for up to 6 months.

#### 2.4. Fluorescence Spectroscopy

Equilibrium binding experiments were performed on a Cary Eclipse Fluorescence Spectrophotometer (Agilent Technologies, Santa Clara, CA, USA). Samples were maintained at 25 °C with a PCB 1500 water peltier system (Agilent). FANCJ peptide (5 µM) was placed in a microcuvette. Fluorescence spectra were collected from 300 nm to 450 nm ( $\lambda_{\text{excitation}} = 280 \text{ nm}$ ) with slit widths set to 5 nm. A scan of Buffer H was used as a baseline. DNA substrate was titrated into the cuvette, and each mixture was equilibrated for 3 min prior to data collection. The extent of fluorescence quenching observed ( $\Delta F_{\text{obs}}$ ) was calculated using the following equation, where  $F_0$  was the total fluorescence signal from the FANCJ peptide alone, and  $F_i$  was the total fluorescence intensity upon the *i*th addition of DNA:

$$\Delta F_{\text{obs}} = \frac{F_0 - F_i}{F_0} \quad (1)$$

Binding isotherms were generated by plotting  $\Delta F_{\text{obs}}$  versus the total DNA concentration after correcting for sample dilution. The resulting curves were fit to a 1:1 interaction model using Scientist 3.0 software (Micromath, St. Louis, MO, USA) based on the following formulas, where  $A$  was the amplitude of fluorescence quenching and  $K$  was the equilibrium association constant.  $D_f$  and  $D_t$  were the free and total concentration of DNA, while  $P_f$  and  $P_t$  described the free and total peptide concentration. Fluorescence titrations were performed in triplicate. The reported values were determined from the average and 95% confidence interval of the three independent data-sets.

$$\Delta F_{obs} = A \left( \frac{KD_f}{1 + KD_f} \right) \quad (2)$$

$$D_t = D_f(1 + KP_f) \quad (3)$$

$$P_t = P_f(1 + KD_f) \quad (4)$$

### 2.5. Circular Dichroism (CD)

CD measurements were collected on a JASCO J-810 spectropolarimeter (JASCO Inc., Easton, MD, USA) equipped with a PTC-423S peltier system. G4 DNA samples were dialyzed into 20 mM Boric Acid pH 7.5, 150 mM KCl (or NaCl). CD spectra were collected from 320 nm to 220 nm at 25 °C. Five traces were obtained for each DNA substrate, and a reference scan of the buffer alone was subtracted from the averaged CD signal.

### 2.6. Biolayer Interferometry (BLI)

BLI assays were performed on a BLItz instrument (Pall Fortébio, Fremont, CA, USA). Streptavidin-coated biosensors were purchased from Pall Fortébio (Lot 1906281). Biosensors were hydrated in Buffer H for 10 min, and the baseline optical interference was recorded. A total of 150 nM of biotinylated G4 DNA or FANCJ PIP peptide was loaded onto the sensors over 2 min, after which they were washed with Buffer H. Binding reactions were initiated by placing the biosensors in analyte solutions at the indicated concentrations. After their interactions had reached an equilibrium, the sensors were returned to buffer to monitor dissociation of the complexes. Experiments were repeated in triplicate. BLI binding isotherms were generated by plotting the plateau values of the association phase versus total analyte concentration. These curves were fit to a 1:1 interaction model, as described above. The parameters reported were obtained from the average and 95% confidence interval of the three data sets.

### 2.7. Data Repository

All raw and processed data files, protocols, and mathematical models used in this work can be accessed freely on the Open Science Framework.

## 3. Results

### 3.1. FANCJ AKKQ Binds to G4 DNA

To test whether the FANCJ AKKQ motif alone can target G4 structures, we used fluorescence spectroscopy to monitor the binding interactions between an FANCJ peptide and a G4 formed by the human telomeric sequence (TTAGGG)<sub>4</sub>. A tryptophan residue was substituted for tyrosine at the C-terminal end of SPEKTTLAAKLSAKKQASIW (FANCJ amino acids 128–147) to serve as a reporter (Figure 1A). The free peptide produced a fluorescence peak from 300 to 450 nm; equilibrium titrations of (TTAGGG)<sub>4</sub> quenched this signal with increasing DNA concentration (Figure 1B). The extent of fluorescence quenching was used to generate a binding isotherm (Figure 1C). Nonlinear least squares analysis of this curve to a single-site interaction model resulted in an affinity value of  $K = 1.6 \pm 0.7 \times 10^6 \text{ M}^{-1}$  (20 mM HEPES pH 7.5, 150 mM KCl, 5 mM TCEP, and 5% (v/v) glycerol, 25 °C). We next examined how the incorporation of 8-oxoguanine affected the FANCJ AKKQ-G4 interactions. 8oxoG4 substrates with a damaged base at the first (8oxo1) or fifth (8oxo5) guanine position were used for fluorescence titrations. These sites were of interest because previous experiments showed they reduced the thermal stability of the human telomeric quadruplex modestly ( $\Delta T_{m,8oxo1} = -12.3 \text{ °C}$ ) or severely ( $\Delta T_{m,8oxo5} = -30.5 \text{ °C}$ ) [44,57]. The FANCJ AKKQ peptide bound to both 8oxoG4s with similar affinities as the native substrate, with  $K_{8oxo1} = 1.3 \pm 0.4 \times 10^6 \text{ M}^{-1}$  and  $K_{8oxo5} = 1.4 \pm 0.5 \times 10^6 \text{ M}^{-1}$  (Figure 1D). However, all three DNA sequences adopted distinct struct folds. CD spectroscopy

confirmed that (TTAGGG)<sub>4</sub> folded into a hybrid conformation, as expected, with a CD peak at ~290 nm, a shoulder at ~260 nm, and a trough near 240 nm (Figure 1E) [4]. The 8oxo1 and 8oxo5 modifications perturbed the G4 structure and shifted its characteristic CD profile (see also Figure S1). These sites were located within different tetrads of the G4 DNA (Figure 1F). The equilibrium binding and CD results suggested that the FANCI AKKQ targeted the TTA loops of (TTAGGG)<sub>4</sub>, since 8-oxoguanine altered the hybrid G4 configuration but had a negligible effect on peptide binding.

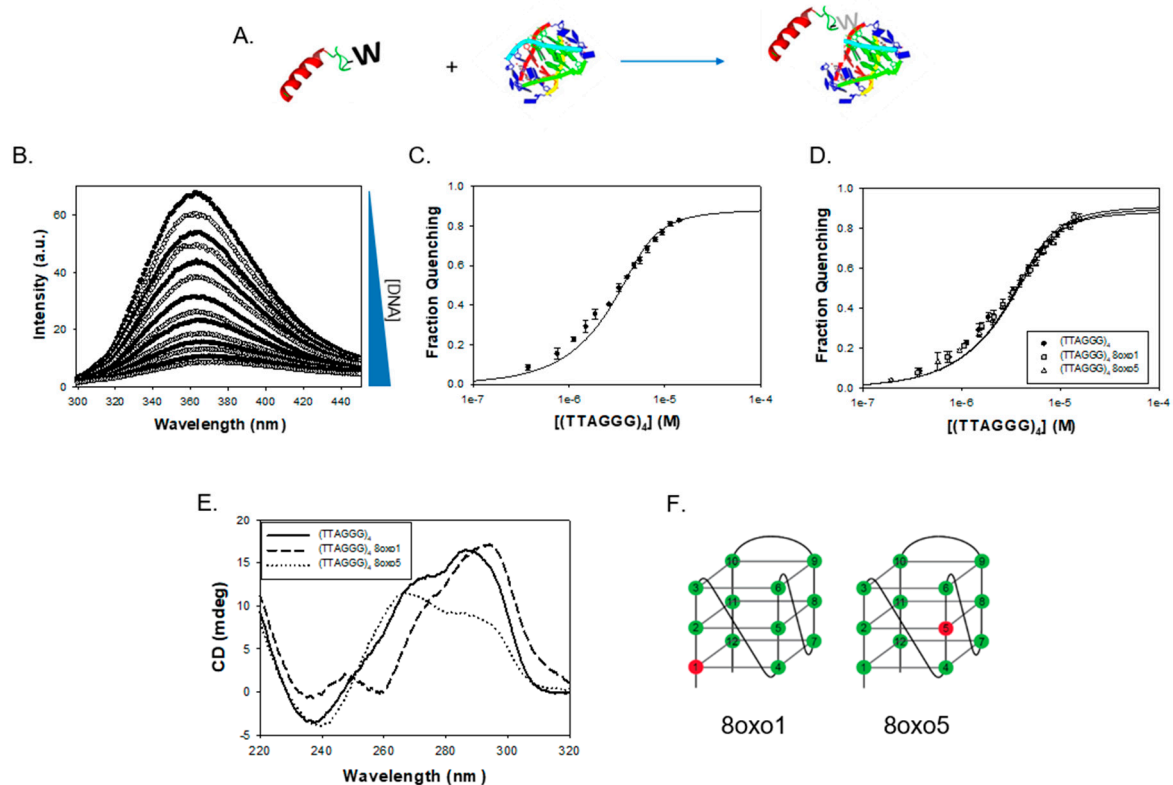


**Figure 1.** (A) Fluorescence spectroscopy was used to study FANCI AKKQ-G4 binding. A tryptophan residue was incorporated into the AKKQ peptide as a fluorescence probe. (B) The peptide produced a large fluorescence peak alone in Buffer H (20 mM HEPES pH 7.5, 150 mM KCl, 5 mM TCEP, and 5% (v/v) glycerol, 25 °C). This signal was quenched upon titration of the human telomeric G4 (TTAGGG)<sub>4</sub>. (C) The extent of fluorescence quenching was plotted against total DNA concentration to generate a binding isotherm. Nonlinear least squares analysis of this curve to a 1:1 binding model resulted in an affinity value of  $K = 1.6 \pm 0.7 \times 10^6 \text{ M}^{-1}$ . (D) Experiments were repeated with 8oxoG-modified substrates at the first (8oxo1) or fifth (8oxo5) guanine position. FANCI AKKQ bound to the damaged G4s with similar affinities, with  $K_{8oxo1} = 1.3 \pm 0.4 \times 10^6 \text{ M}^{-1}$  and  $K_{8oxo5} = 1.4 \pm 0.5 \times 10^6 \text{ M}^{-1}$ . (E) Circular dichroism spectra of the native (TTAGGG)<sub>4</sub> confirmed formation of a hybrid G4 structure (solid line). The 8oxo1 (dashed line) and 8oxo5 (dotted dash) substrates disrupted G4-folding. (F) Schematic representation of a hybrid G4, formed by (TTAGGG)<sub>4</sub>. The 12 guanines within the sequence are numbered, and the damaged DNA sites of interest are highlighted in red.

We therefore hypothesized that a G4 substrate with shorter connecting loops between the quartets would allow FANCI AKKQ to better “sense” DNA damage. To test this, we monitored the binding of the peptide and a quadruplex formed by (GGGT)<sub>4</sub> with 8-oxoguanine at the corresponding 8oxo1 and 8oxo5 positions. This sequence was chosen because the single thymidine spacers produced a compact parallel G4 with high thermal stability ( $T_m = \sim 85 \text{ °C}$ ) [58]. FANCI AKKQ bound to (GGGT)<sub>4</sub> with lowered affinity  $K = 2.7 \pm 0.4 \times 10^5 \text{ M}^{-1}$  compared to (TTAGGG)<sub>4</sub>. The presence of oxidative damage, however, increased the equilibrium constant values ~1.5–3 fold, with  $K_{8oxo1} = 7.7 \pm 0.7 \times 10^5 \text{ M}^{-1}$  and  $K_{8oxo5} = 4.4 \pm 0.6 \times 10^5 \text{ M}^{-1}$  (Figure 2A). CD analysis of (GGGT)<sub>4</sub> indicated the formation of a

parallel G4, which had a CD maximum at ~265 nm and a minimum at ~245 nm [4]. The incorporation of 8-oxoguanine did not affect G4-folding (Figure 2B). All three DNA sequences retained a parallel conformation. These results were consistent with our working model. The thymidine handles on (GGGT)<sub>4</sub> limited contacts available to the peptide and decreased its affinity for the G4. This also freed FANCI AKKQ to bind directly to the damaged DNA sites within the 8oxo1 and 8oxo5 substrates. A summary of the equilibrium binding parameters is provided in Table 2, below.

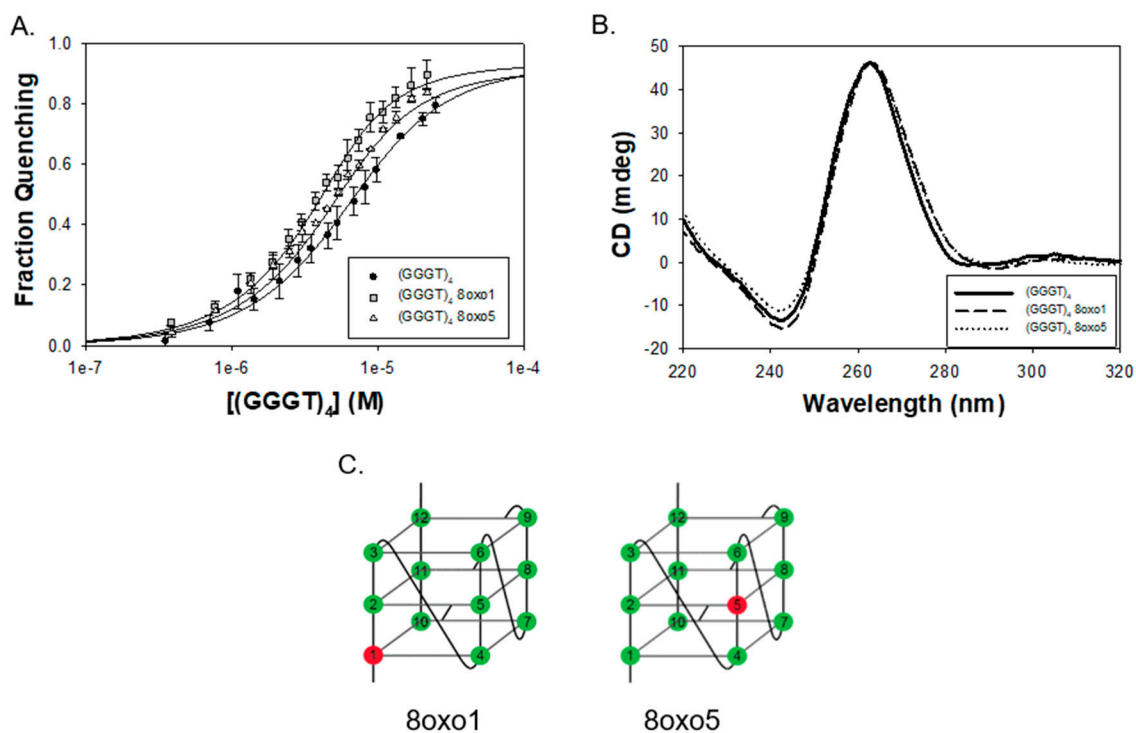


**Figure 2.** (A) Fluorescence spectroscopy results of FANCI AKKQ binding to (GGGT)<sub>4</sub> and substrates with 8oxoG at the first (8oxo1) or fifth (8oxo5) guanine position. Nonlinear least squares of the binding isotherms to a one-site interaction model resulted in  $K = 2.7 \pm 0.4 \times 10^5 \text{ M}^{-1}$ ,  $K_{8oxo1} = 7.7 \pm 0.7 \times 10^5 \text{ M}^{-1}$ , and  $K_{8oxo5} = 4.4 \pm 0.6 \times 10^5 \text{ M}^{-1}$ . (B) Circular dichroism spectra of the undamaged (GGGT)<sub>4</sub> indicated formation of a parallel G4 structure (solid line). Incorporation of 8oxoG at the 8oxo1 (dashed line) and 8oxo5 (dotted dash) sites had no effect on G4-folding. (C) Cartoon diagram of a parallel G4 formed by (GGGT)<sub>4</sub>. The guanines within the sequence are labeled, and the damaged DNA sites of interest in this work are shown in red.

**Table 2.** Summary of FANCI AKKQ-G4 binding results by fluorescence spectroscopy.

DNA Sequence	$K \text{ (M}^{-1}\text{)}$	A	$R^2$
(TTAGGG) <sub>4</sub>	$1.6 \pm 0.7 \times 10^6$	$0.88 \pm 0.05$	0.9961
(TTAGGG) <sub>4</sub> 8oxo1	$1.3 \pm 0.4 \times 10^6$	$0.90 \pm 0.04$	0.9974
(TTAGGG) <sub>4</sub> 8oxo5	$1.4 \pm 0.5 \times 10^6$	$0.91 \pm 0.05$	0.9967
(GGGT) <sub>4</sub>	$2.7 \pm 0.4 \times 10^5$	$0.93 \pm 0.04$	0.9977
(GGGT) <sub>4</sub> 8oxo1	$7.7 \pm 0.7 \times 10^5$	$0.93 \pm 0.01$	0.9988
(GGGT) <sub>4</sub> 8oxo5	$4.4 \pm 0.6 \times 10^5$	$0.91 \pm 0.03$	0.9972

### 3.2. An Optical Biosensor for AKKQ-G4 Binding

We next validated our fluorescence spectroscopy results by biolayer interferometry (BLI). This technique measures the optical thickness of a biosensor surface, which can be used to examine the association and dissociation reactions of macromolecules [59–61]. In BLI, an incident white light passes through a biosensor, and the interference pattern of the reflected light is directly proportional

to the thickness of the sensor tip (Figure 3A). When a molecule of interest is bound to the surface, the increased distance traveled by the incident light before it is reflected produces a wavelength shift ( $\Delta\lambda$ ) in the optical interference. Hence, when a binding partner for the immobilized target is added, the formation of their complex will further increase  $\Delta\lambda$  or vice versa upon their dissociation. In our studies, biotinylated human telomeric G4 DNA was placed on a streptavidin-coated BLI biosensor (Figure 3B). The optical interference pattern of the sensor alone was measured in Buffer H as an initial baseline (phase 1). DNA substrate was loaded on the sensor tip, and an increase in  $\Delta\lambda$  was observed (phase 2). The sensor was then washed with Buffer H to establish a new baseline signal and to confirm that the G4 remained bound onto the surface (phase 3). FANCI AKKQ was introduced to initiate the association reaction (phase 4). After a binding equilibrium was reached, the sensor was placed in Buffer H to monitor their dissociation (phase 5). BLI experiments were performed as a function of FANCI AKKQ concentration, and the resulting time-courses in Figure 3C were truncated to show only the association and dissociation phases (full traces are provided in Figure S2). The plateau  $\Delta\lambda$  values at the end of the binding phase were plotted against peptide concentration to generate an isotherm; nonlinear least squares analysis of this curve to a 1:1 interaction model resulted in an equilibrium constant of  $K = 9.4 \pm 1.1 \times 10^4 \text{ M}^{-1}$  (Figure 3D). BLI experiments with biotinylated 8oxoG4s showed a small increase in affinity in the presence of DNA damage, with  $K_{8oxo1} = 2.3 \pm 0.8 \times 10^5 \text{ M}^{-1}$  and  $K_{8oxo5} = 1.8 \pm 0.2 \times 10^5 \text{ M}^{-1}$ . These binding constants were about one order of magnitude weaker compared to the fluorescence measurements. Since the DNA was immobilized for BLI, its surface orientation on the sensor may have occluded peptide binding. This would reduce the overall affinity but enable FANCI to interact directly with the damaged base in the 8oxo1 and 8oxo5 G4 substrates. BLI results are summarized in Table 3 below.

**Table 3.** Summary of AKKQ-G4 binding results by biolayer interferometry.

DNA Sequence	K ( $\text{M}^{-1}$ )	A	R <sup>2</sup>
bioPEG12-(TTAGGG) <sub>4</sub>	$9.4 \pm 1.1 \times 10^4$	$0.74 \pm 0.03$	0.9973
bioPEG12-(TTAGGG) <sub>4</sub> -8oxo1	$2.3 \pm 0.8 \times 10^5$	$0.49 \pm 0.06$	0.9807
bioPEG12-(TTAGGG) <sub>4</sub> -8oxo5	$1.8 \pm 0.2 \times 10^5$	$0.69 \pm 0.03$	0.9954

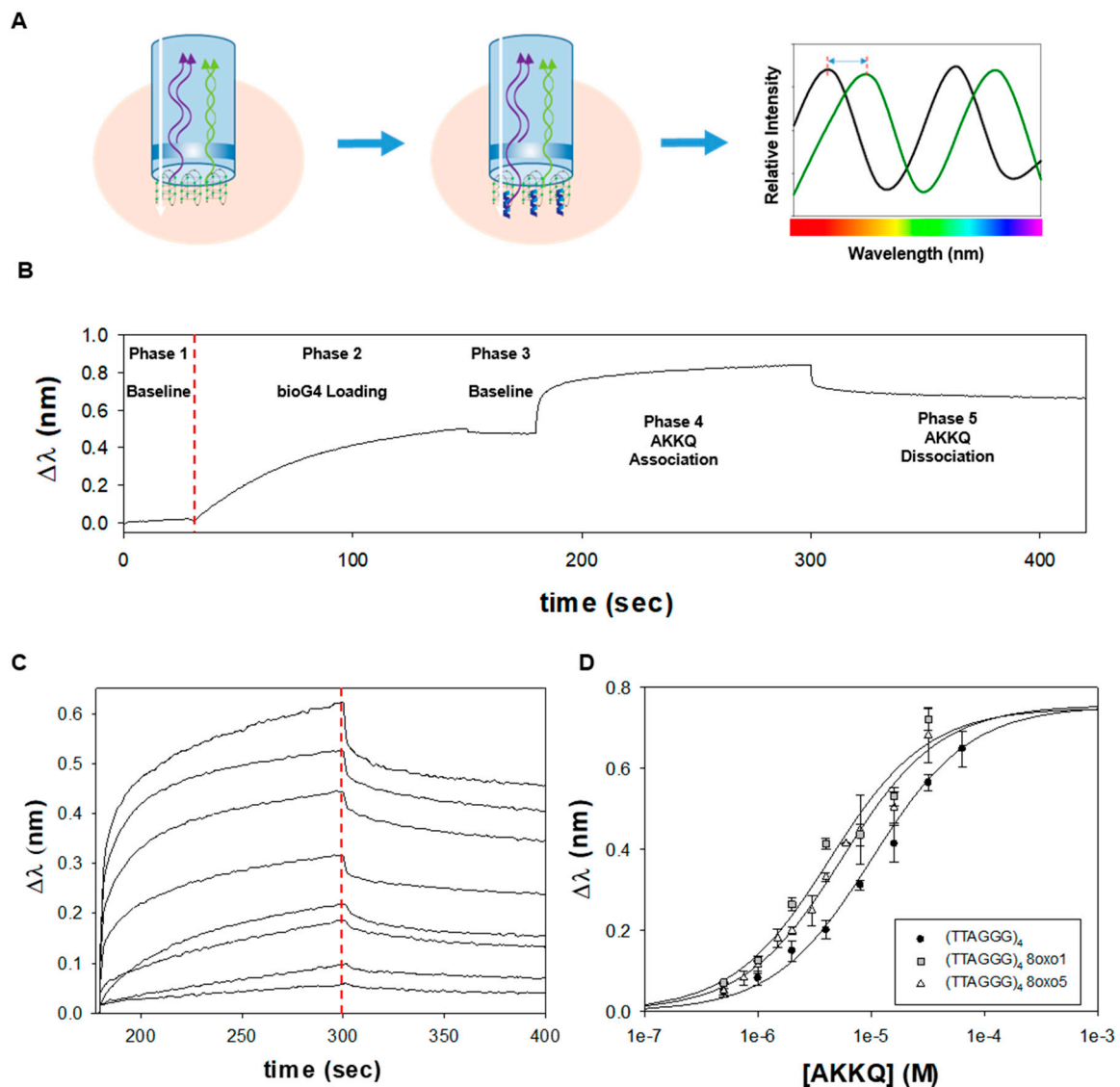


**Figure 3.** (A) Biolayer interferometry (BLI) overview. BLI measures the thickness of an optical surface. When an incident white light passes through a biosensor, the interference pattern of the reflected light is dependent on the distance traveled by the beam. When a molecule binds to the surface, a wavelength shift in the optical interference ( $\Delta\lambda$ ) is measured in real-time by the BLI instrument. This signal is used to report the association or dissociation of molecular complexes. (B) In a typical BLI trajectory, the interference pattern of a streptavidin-coated biosensor was measured in Buffer H to establish a baseline optical signal (phase 1). Biotinylated human telomeric G4 DNA was loaded onto the sensor tip through biotin-streptavidin interactions and an increase in  $\Delta\lambda$  was measured (phase 2). The biosensor was washed with buffer to confirm the DNA substrate remained surface-immobilized (phase 3). Freely diffusing FANCI AKKQ peptide was introduced to initiate the association reaction (phase 4). Once a binding equilibrium was reached, the biosensor was placed in buffer to examine the dissociation of AKKQ-G4 complexes. (C) BLI experiments were performed in triplicate as a function of FANCI AKKQ peptide concentration (64, 32, 16, 8, 4, 2, 1, and 0.5  $\mu\text{M}$ ). Time-courses were truncated to show the binding and dissociation phases. (D) The equilibrium  $\Delta\lambda$  values at the end of the association phase were plotted against AKKQ concentration to construct a binding isotherm. Fitting this curve to a one-site interaction model yielded  $K = 9.4 \pm 1.1 \times 10^4 \text{ M}^{-1}$ . BLI experiments with an 8oxo1 or 8oxo5 modification within  $(\text{TTAGGG})_4$  resulted in small increases in affinity, with  $K_{8\text{oxo}1} = 2.3 \pm 0.8 \times 10^5 \text{ M}^{-1}$  and  $K_{8\text{oxo}5} = 1.8 \pm 0.2 \times 10^5 \text{ M}^{-1}$ .

### 3.3. FANCI PIP Recruits REV1 and PCNA

It was suggested that FANCI possessed a PCNA-interaction peptide (PIP) within amino acids 1001–1017 (SWSSFNSLGGYFTGKIP), based on the underlined consensus residues [42]. PIP-containing proteins bind directly to PCNA to coordinate DNA replication and repair [53,62,63]. However, it is now evident that noncanonical PIP-boxes can serve as hotspots to recruit other proteins, including the REV1 translesion synthesis polymerase and the MLH1 mismatch repair protein [54–56,64]. To test if the PIP-like motif in FANCI functions as a PIP or an REV1-interacting region (RIR), we compared how this peptide bound to PCNA versus REV1 by BLI. Recombinant human PCNA protein and the C-terminal domain (CTD) of human REV1 were purified from *E. coli* (Figure S3A) [54]. Biotinylated FANCI PIP was immobilized on a streptavidin-coated biosensor and experiments were performed as described above. As seen in the truncated time-courses, REV1 CTD produced a larger binding signal than PCNA at similar molar concentrations of protein (Figure 4A). Because  $\Delta\lambda$  is related to the thickness of the bilayer, this value reports the accumulation of mass on the sensor tip. Hence, our BLI results indicated that more REV1 CTD molecules bound to the FANCI PIP than PCNA. This difference is further magnified as REV1 CTD has a molecular mass of ~12 kDa, while a human PCNA trimer is about seven times its size, at ~86 kDa [65,66]. Next, we tested the effects of a FANCI PIP AA peptide on its interactions with REV1 CTD and PCNA. The consecutive consensus aromatic residues (YF) within the potential PIP-motif were replaced with alanine amino acids (AA). To our surprise, BLI time-courses of FANCI PIP AA also showed that more REV1 CTD bound to the mutant peptide versus PCNA (Figure 4B). In fact, an overlay of the trajectories revealed that PIP AA produced larger binding signals compared to the wild-type PIP sequence for REV1 CTD (Figure 4C) and for PCNA (Figure 4D). BLI experiments with PIP and PIP AA were repeated as a function of REV1 CTD and PCNA concentration to measure their corresponding equilibrium constant values. The PIP AA mutation resulted in a small increase in affinity for REV1 CTD (Figure S3B and S3C) but the binding of PCNA was weakened twofold (Figure S3D and S3E). Our results suggest that the PIP sequence in FANCI has the biochemical properties of a canonical PIP-box that binds to PCNA, but it functions better as an RIR-motif that interacts with the REV1 polymerase.

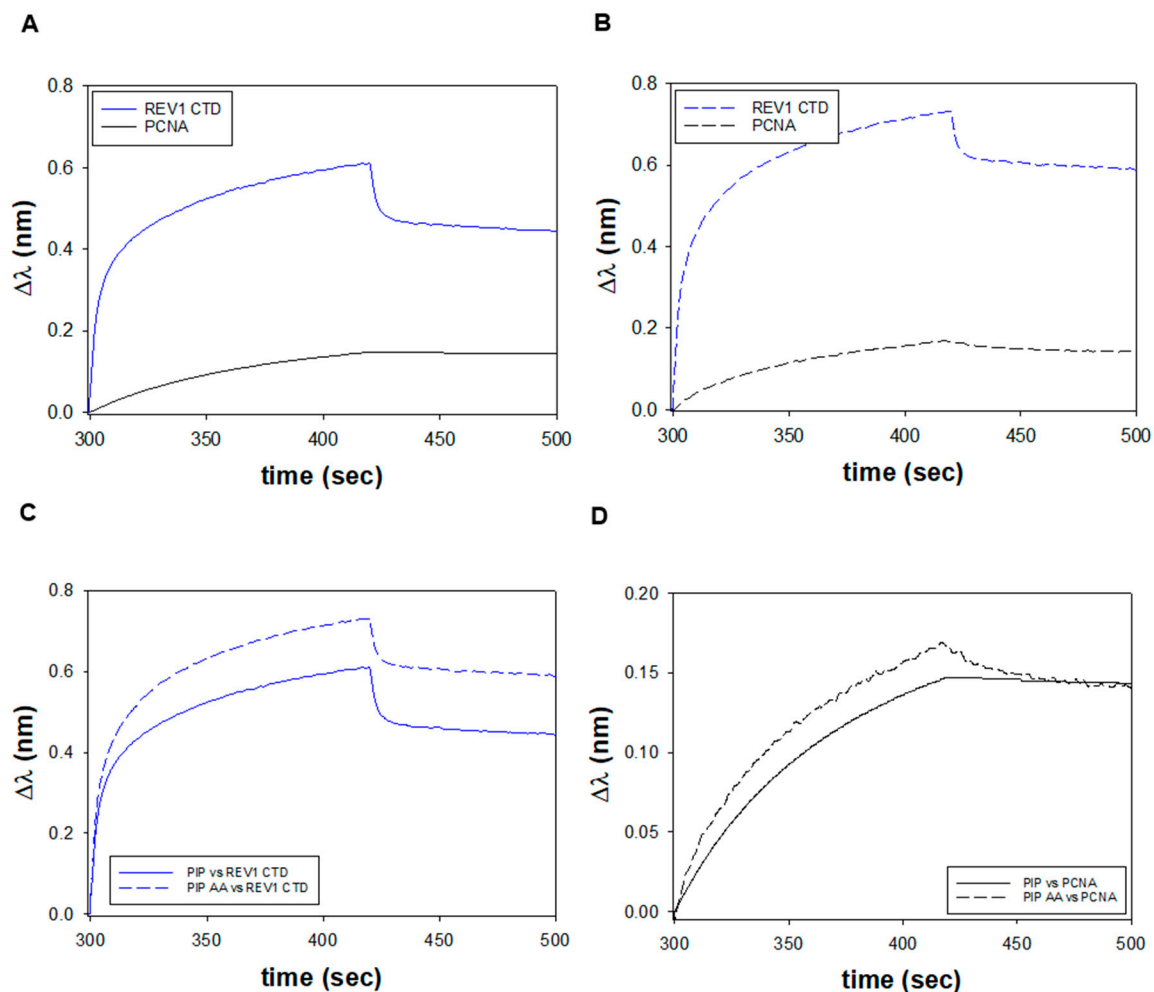


**Figure 4.** (A) BLI time-courses of a biotinylated FANCJ PIP (150 nM), binding to either 1.8  $\mu$ M REV1 CTD (solid blue) or 1.3  $\mu$ M PCNA trimer (solid black). (B) BLI experiments with biotinylated FANCJ PIP AA (150 nM) and REV1 CTD (dashed blue) versus PCNA (dashed black). (C) Overlay of the data from panels A and B for REV1 CTD with FANCJ PIP (solid blue) or PIP AA (dashed blue). (D) Overlay of the data from panels A and B for PCNA with the wild-type (solid black) versus the mutant FANCJ peptide (dashed black).

#### 4. Discussion

Our fluorescence spectroscopy and BLI results indicate that the FANCJ AKKQ peptide alone can bind to G4s and 8oxoG4s. Hence, this site may be crucial for the molecular recognition of damaged G4s inside the cell. This is consistent with a previous study, in which K141/142A mutations of FANCJ AKKQ abrogated G4 binding completely [42]. Structural determinants of the interactions between FANCJ AKKQ and 8oxoG4s are currently being tested in our laboratory. We initially predicted that the incorporation of 8oxoG would destabilize G4s and that the AKKQ peptide may have a greater affinity for these structures. To our surprise, the CD measurements and binding data led to a different result. The human telomeric G4 (TTAGGG)<sub>4</sub> adopted a hybrid conformation in KCl-containing buffer, and 8oxoG modifications at the 8oxo1 and 8oxo5 positions disrupted G4-folding as anticipated [44]; however, FANCJ AKKQ had the same affinity for 8oxoG4s as the native substrate. It was observed also by NMR that 8oxoG within the human telomeric G4 converted guanine glycosidic angles from *anti* to *syn* and changed the G4 configuration [43]. So how can FANCJ bind to an undamaged G4 with the same affinity as 8oxo1/5 when all three substrates folded into distinct forms? We reasoned that FANCJ AKKQ bound specifically to the TTA loop of the (TTAGGG)<sub>4</sub> sequence, which would explain

why the peptide was insensitive to the presence of 8oxoG in the rest of the quadruplex. Indeed, CD and binding results with a G4 formed by (GGGT)<sub>4</sub> were consistent with this model. By shortening the loops that connect adjacent guanine tetrads to a single thymidine, the physical contacts available to FANCI were limited, which reduced its overall affinity for this substrate. However, because AKKQ was no longer sequestered by the loop, the peptide could target the damaged base and we observed higher equilibrium constant values for FANCI AKKQ binding to 8oxo1/5 for (GGGT)<sub>4</sub> (Figure 5).

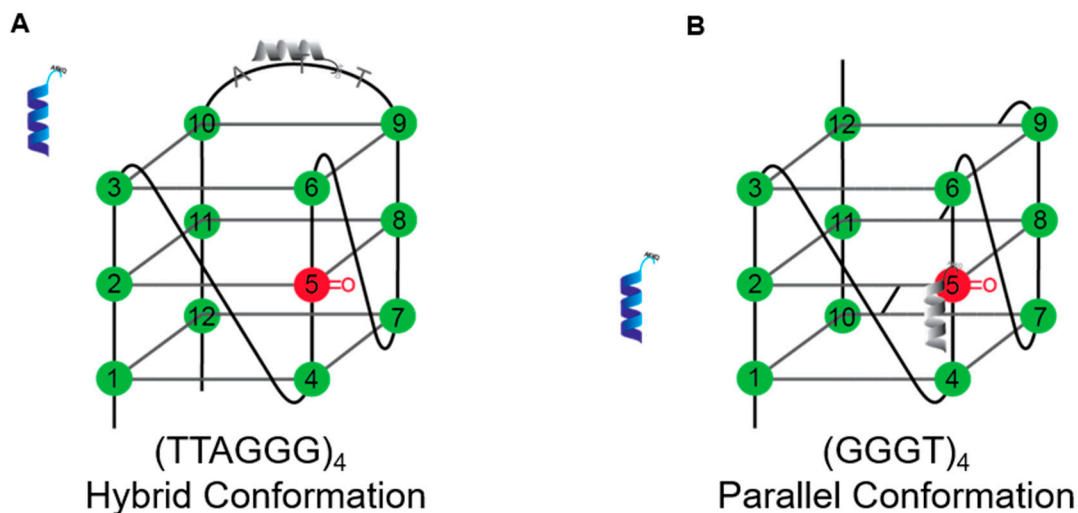


**Figure 5.** Model for 8oxoG4 recognition by FANCI AKKQ. (A) The human telomeric G4 DNA (TTAGGG)<sub>4</sub> adopts a hybrid configuration. The FANCI AKKQ peptide binds with high affinity to the TTA loop and does not interact with an 8oxoG-modified base. Partial unfolding or rearrangement of this structure would therefore have no impact on the AKKQ-G4 interaction. (B) (GGGT)<sub>4</sub> folds into a parallel G4. The shortened loops reduced its affinity for FANCI AKKQ, which enabled the peptide to interact directly with a surface-exposed 8oxoG.

Classical PIP-boxes bind to PCNA, which is a strategy used to recruit repair polymerases to damaged DNA sites [53]. Because PCNA forms a trimeric ring, it can carry up to three different repair enzymes through PIP interactions as a molecular tool belt [67]. This would enable the complex to switch polymerases in order to bypass damage-specific lesions. It has been shown that some PIP-like sequences can serve as hotspots to bind directly to other repair proteins without the need for a PCNA hub [54,68]. FANCI possesses a potential PIP-motif based on its primary amino acid sequence [42,56]. Our BLI analysis showed that the FANCI PIP bound to REV1 CTD and to PCNA. Interactions with REV1 CTD, however, produced a stronger binding signal than PCNA, suggesting that the formation of a PIP-CTD complex was more favorable. Interestingly, the PIP AA mutant reduced the binding constant for PCNA by half but resulted in a small increase in affinity for REV1 CTD. Corresponding double alanine substitutions within the PIP motifs of Polη and Polι have eliminated PCNA binding entirely [69]. Since FANCI PIP AA still retained residual interactions with PCNA, it likely does not function as a canonical PIP-box. Similar mutations in RIRs have either reduced or prevented binding of REV1 [54,68]. Taken together, the FANCI PIP has biochemical properties of PIPs and RIRs, but the consecutive aromatic amino acids within the broadly defined PIP consensus sequence are disposable for protein binding. It is possible that protein-protein interactions are mediated by an upstream phenylalanine residue (shown in red) of the site (SWSSFNSLQYFTGKIP), as seen in some APIM motifs [70]. Having a PIP-box that can bind to both PCNA and REV1 may indicate that FANCI forms a ternary complex with both proteins to process G4s. Our current research focus is using BLI to pre-form a PIP-PCNA or PIP-CTD complex, and then examining the binding interactions of the third partner. We also plan on recapitulating the G4 and protein binding activities presented here, using full-length proteins in order to reconstitute a functional G4-repair complex.

**Supplementary Materials:** The following are available online at <http://www.mdpi.com/2073-4425/11/1/5/s1>, Figure S1: CD spectra of (TTAGGG)<sub>4</sub> and (GGGT)<sub>4</sub> in Buffer H with 150 mM NaCl, Figure S2: BLI time-courses of the FANCJ AKKQ peptide binding to 8oxoG4s, Figure S3: BLI binding experiments with FANCJ PIP, REV1 CTD, and PCNA.

**Author Contributions:** Conceptualization, K.L. and C.G.W.; methodology, C.G.W.; software, K.L., L.C., and P.P.; validation, K.L., L.C., P.P., and C.G.W.; formal analysis, K.L., L.C., and C.G.W.; investigation, K.L., L.C., and P.P.; resources, C.G.W.; data curation, K.L., L.C., P.P., and C.G.W.; writing—original draft preparation, K.L. and C.G.W.; writing—review and editing, K.L., L.C., P.P., and C.G.W.; visualization, K.L., L.C., P.P., and C.G.W.; supervision, K.L. and C.G.W.; project administration, C.G.W.; funding acquisition, C.G.W. All authors have read and agreed to the published version of the manuscript.

**Funding:** This research was funded by the American Heart Association, grant number 17AIREA33661285 to C.G.W.

**Acknowledgments:** We thank Michael D. Sevilla and members of the Wu Laboratory at Oakland University for their comments on this manuscript and for their valuable scientific discussions. The pEB022 plasmid used to produce full-length human PCNA protein was a generous gift from M. Todd Washington at the University of Iowa.

**Conflicts of Interest:** The authors declare no conflict of interest.

## References

1. Bochman, M.L.; Paeschke, K.; Zakian, V.A. DNA secondary structures: Stability and function of G-quadruplex structures. *Nat. Rev. Genet.* **2012**, *13*, 770–780. [[CrossRef](#)] [[PubMed](#)]
2. Hao, F.; Ma, Y.; Guan, Y. Effects of Central Loop Length and Metal Ions on the Thermal Stability of G-Quadruplexes. *Molecules* **2019**, *24*, 1863. [[CrossRef](#)] [[PubMed](#)]
3. Burge, S.; Parkinson, G.N.; Hazel, P.; Todd, A.K.; Neidle, S. Quadruplex DNA: Sequence, topology and structure. *Nucleic Acids Res.* **2006**, *34*, 5402–5415. [[CrossRef](#)] [[PubMed](#)]
4. Del Villar-Guerra, R.; Trent, J.O.; Chaires, J.B. G-Quadruplex Secondary Structure Obtained from Circular Dichroism Spectroscopy. *Angew. Chem. Int. Ed. Engl.* **2018**, *57*, 7171–7175. [[CrossRef](#)] [[PubMed](#)]
5. Rhodes, D.; Lipps, H.J. G-quadruplexes and their regulatory roles in biology. *Nucleic Acids Res.* **2015**, *43*, 8627–8637. [[CrossRef](#)] [[PubMed](#)]
6. Siddiqui-Jain, A.; Grand, C.L.; Bearss, D.J.; Hurley, L.H. Direct evidence for a G-quadruplex in a promoter region and its targeting with a small molecule to repress c-MYC transcription. *Proc. Natl. Acad. Sci. USA* **2002**, *99*, 11593–11598. [[CrossRef](#)]
7. Song, J.; Perreault, J.P.; Topisirovic, I.; Richard, S. RNA G-quadruplexes and their potential regulatory roles in translation. *Translation* **2016**, *4*, e1244031. [[CrossRef](#)]
8. Wolfe, A.L.; Singh, K.; Zhong, Y.; Drewe, P.; Rajasekhar, V.K.; Sanghvi, V.R.; Mavrakis, K.J.; Jiang, M.; Roderick, J.E.; van der Meulen, J.; et al. RNA G-quadruplexes cause eIF4A-dependent oncogene translation in cancer. *Nature* **2014**, *513*, 65–70. [[CrossRef](#)]
9. Bidzinska, J.; Cimino-Reale, G.; Zaffaroni, N.; Folini, M. G-Quadruplex Structures in the Human Genome as Novel Therapeutic Targets. *Molecules* **2013**, *18*, 12368–12395. [[CrossRef](#)]
10. Marin-Garcia, J. Mitochondrial DNA repair: A novel therapeutic target for heart failure. *Heart Fail. Rev.* **2016**, *21*, 475–487. [[CrossRef](#)]
11. Neidle, S. Quadruplex Nucleic Acids as Novel Therapeutic Targets. *J. Med. Chem.* **2016**, *59*, 5987–6011. [[CrossRef](#)] [[PubMed](#)]
12. Wu, Y.; Shin-ya, K.; Brosh, R.M. FANCJ helicase defective in Fanconia anemia and breast cancer unwinds G-quadruplex DNA to defend genomic stability. *Mol. Cell. Biol.* **2008**, *28*, 4116–4128. [[CrossRef](#)] [[PubMed](#)]
13. Zhou, B.; Geng, Y.; Liu, C.; Miao, H.; Ren, Y.; Xu, N.; Shi, X.; You, Y.; Lee, T.; Zhu, G. Characterizations of distinct parallel and antiparallel G-quadruplexes formed by two-repeat ALS and FTD related GGGGCC sequence. *Sci. Rep.* **2018**, *8*, 2366. [[CrossRef](#)] [[PubMed](#)]
14. Wu, Y.; Brosh, R.M. G-quadruplex nucleic acids and human disease. *FEBS J.* **2010**, *277*, 3470–3488. [[CrossRef](#)] [[PubMed](#)]
15. Chambers, V.S.; Marsico, G.; Boutell, J.M.; di Antonio, M.; Smith, G.P.; Balasubramanian, S. High-throughput sequencing of DNA G-quadruplex structures in the human genome. *Nat. Biotechnol.* **2015**, *33*, 877–881. [[CrossRef](#)] [[PubMed](#)]

16. Marsico, G.; Chambers, V.S.; Sahakyan, A.B.; McCauley, P.; Boutell, J.M.; Antonio, M.D.; Balasubramanian, S. Whole genome experimental maps of DNA G-quadruplexes in multiple species. *Nucleic Acids Res.* **2019**, *47*, 3862–3874. [[CrossRef](#)] [[PubMed](#)]
17. Castillo Bosch, P.; Segura-Bayona, S.; Koole, W.; van Heteren, J.T.; Dewar, J.M.; Tijsterman, M.; Knipscheer, P. FANCI promotes DNA synthesis through G-quadruplex structures. *EMBO J.* **2014**, *33*, 2521–2533. [[CrossRef](#)]
18. Eddy, S.; Ketkar, A.; Zafar, M.K.; Maddukuri, L.; Choi, J.Y.; Eoff, R.L. Human Rev1 polymerase disrupts G-quadruplex DNA. *Nucleic Acids Res.* **2014**, *42*, 3272–3285. [[CrossRef](#)]
19. Budhathoki, J.B.; Ray, S.; Urban, V.; Janscak, P.; Yodh, J.G.; Balci, H. RecQ-core of BLM unfolds telomeric G-quadruplex in the absence of ATP. *Nucleic Acids Res.* **2014**, *42*, 11528–11545. [[CrossRef](#)]
20. Vannier, J.B.; Pavicic-Kaltenbrunner, V.; Petalcorin, M.I.; Ding, H.; Boulton, S.J. RTEL1 dismantles T loops and counteracts telomeric G4-DNA to maintain telomere integrity. *Cell* **2012**, *149*, 795–806. [[CrossRef](#)]
21. Sanders, C.M. Human Pif1 helicase is a G-quadruplex DNA-binding protein with G-quadruplex DNA-unwinding activity. *Biochem. J.* **2010**, *430*, 119–128. [[CrossRef](#)] [[PubMed](#)]
22. Wu, G.; Xing, Z.; Tran, E.J.; Yang, D. DDX5 helicase resolves G-quadruplex and is involved in MYC gene transcriptional activation. *Proc. Natl. Acad. Sci. USA* **2019**, *116*, 20453–20461. [[CrossRef](#)] [[PubMed](#)]
23. Singh, S.P.; Soranno, A.; Sparks, M.A.; Galletto, R. Branched unwinding mechanism of the Pif1 family of DNA helicases. *Proc. Natl. Acad. Sci. USA* **2019**, *116*, 24533–24541. [[CrossRef](#)] [[PubMed](#)]
24. Voter, A.F.; Callaghan, M.M.; Tippana, R.; Myong, S.; Dillard, J.P.; Keck, J.L. Antigenic variation in *Neisseria gonorrhoeae* occurs independently of RecQ-mediated unwinding of the pilE G-quadruplex. *J. Bacteriol.* **2019**. [[CrossRef](#)]
25. Lohman, T.M.; Bjornson, K.P. Mechanisms of helicase-catalyzed DNA unwinding. *Annu. Rev. Biochem.* **1996**, *65*, 169–214. [[CrossRef](#)]
26. Patel, S.S.; Donmez, I. Mechanisms of Helicases. *J. Biol. Chem.* **2006**, *281*, 18265–18268. [[CrossRef](#)]
27. Steitz, T.A. DNA polymerases: Structural diversity and common mechanisms. *J. Biol. Chem.* **1999**, *274*, 17395–17398. [[CrossRef](#)]
28. Lohman, T.M.; Tomko, E.J.; Wu, C.G. Non-hexameric DNA helicases and translocases: Mechanisms and regulation. *Nat. Rev. Mol. Cell Biol.* **2008**, *9*, 391–401. [[CrossRef](#)]
29. Wu, C.G.; Spies, M. Overview: What Are Helicases? In *DNA Helicases and DNA Motor Proteins*; Springer: New York, NY, USA, 2013; pp. 1–16.
30. Bandwar, R.P.; Patel, S.S. The energetics of consensus promoter opening by T7 RNA polymerase. *J. Mol. Biol.* **2002**, *324*, 63–72. [[CrossRef](#)]
31. Cowart, M.; Gibson, K.J.; Allen, D.J.; Benkovic, S.J. DNA substrate structural requirements for the exonuclease and polymerase activities of prokaryotic and phage DNA polymerases. *Biochemistry* **1989**, *28*, 1975–1983. [[CrossRef](#)]
32. Reynolds, K.A.; Cameron, C.E.; Raney, K.D. Melting of Duplex DNA in the Absence of ATP by the NS3 Helicase Domain through Specific Interaction with a Single-Strand/Double-Strand Junction. *Biochemistry* **2015**, *54*, 4248–4258. [[CrossRef](#)] [[PubMed](#)]
33. Wong, C.J.; Lucius, A.L.; Lohman, T.M. Energetics of DNA end binding by *E. coli* RecBC and RecBCD helicases indicate loop formation in the 3′-single-stranded DNA tail. *J. Mol. Biol.* **2005**, *352*, 765–782. [[CrossRef](#)] [[PubMed](#)]
34. van Wietmarschen, N.; Merzouk, S.; Halsema, N.; Spierings, D.C.J.; Guryev, V.; Lansdorp, P.M. BLM helicase suppresses recombination at G-quadruplex motifs in transcribed genes. *Nat. Commun.* **2018**, *9*, 271. [[CrossRef](#)] [[PubMed](#)]
35. Johnson, J.E.; Cao, K.; Ryvkin, P.; Wang, L.S.; Johnson, F.B. Altered gene expression in the Werner and Bloom syndromes is associated with sequences having G-quadruplex forming potential. *Nucleic Acids Res.* **2010**, *38*, 1114–1122. [[CrossRef](#)] [[PubMed](#)]
36. Paeschke, K.; Capra, J.A.; Zakian, V.A. DNA replication through G-quadruplex motifs is promoted by the *Saccharomyces cerevisiae* Pif1 DNA helicase. *Cell* **2011**, *145*, 678–691. [[CrossRef](#)] [[PubMed](#)]
37. Schiavone, D.; Guilbaud, G.; Murat, P.; Papadopoulou, C.; Sarkies, P.; Prioleau, M.N.; Balasubramanian, S.; Sale, J.E. Determinants of G quadruplex-induced epigenetic instability in REV1-deficient cells. *EMBO J.* **2014**, *33*, 2507–2520. [[CrossRef](#)]
38. Lerner, L.K.; Sale, J.E. Replication of G Quadruplex DNA. *Genes* **2019**, *10*, 95. [[CrossRef](#)]

39. Huber, M.D.; Duquette, M.L.; Shiels, J.C.; Maizels, N. A conserved G4 DNA binding domain in RecQ family helicases. *J. Mol. Biol.* **2006**, *358*, 1071–1080. [[CrossRef](#)] [[PubMed](#)]
40. Lattmann, S.; Giri, B.; Vaughn, J.P.; Akman, S.A.; Nagamine, Y. Role of the amino terminal RHAU-specific motif in the recognition and resolution of guanine quadruplex-RNA by the DEAH-box RNA helicase RHAU. *Nucleic Acids Res.* **2010**, *38*, 6219–6233. [[CrossRef](#)]
41. Heddi, B.; Cheong, V.V.; Martadinata, H.; Phan, A.T. Insights into G-quadruplex specific recognition by the DEAH-box helicase RHAU: Solution structure of a peptide-quadruplex complex. *Proc. Natl. Acad. Sci. USA* **2015**, *112*, 9608–9613. [[CrossRef](#)]
42. Wu, C.G.; Spies, M. G-quadruplex recognition and remodeling by the FANCI helicase. *Nucleic Acids Res.* **2016**, *44*, 8742–8753. [[CrossRef](#)] [[PubMed](#)]
43. Bielskute, S.; Plavec, J.; Podbevsek, P. Impact of Oxidative Lesions on the Human Telomeric G-Quadruplex. *J. Am. Chem. Soc.* **2019**, *141*, 2594–2603. [[CrossRef](#)] [[PubMed](#)]
44. Vorlickova, M.; Tomasko, M.; Sagi, A.J.; Bednarova, K.; Sagi, J. 8-oxoguanine in a quadruplex of the human telomere DNA sequence. *FEBS J.* **2012**, *279*, 29–39. [[CrossRef](#)] [[PubMed](#)]
45. Taniguchi, T.; D'Andrea, A.D. Molecular pathogenesis of Fanconi anemia: Recent progress. *Blood* **2006**, *107*, 4223–4233. [[CrossRef](#)]
46. Brosh, R.M.; Cantor, S.B. Molecular and cellular functions of the FANCI DNA helicase defective in cancer and in Fanconi anemia. *Front. Genet.* **2014**, *5*, 372. [[CrossRef](#)]
47. Palovcak, A.; Liu, W.; Yuan, F.; Zhang, Y. Maintenance of genome stability by Fanconi anemia proteins. *Cell Biosci.* **2017**, *7*, 8. [[CrossRef](#)]
48. Datta, A.; Brosh, R.M. Holding All the Cards-How Fanconi Anemia Proteins Deal with Replication Stress and Preserve Genomic Stability. *Genes (Basel)* **2019**, *10*, 170. [[CrossRef](#)]
49. Cantor, S.B.; Xie, J. Assessing the link between BACH1/FANCI and MLH1 in DNA crosslink repair. *Environ. Mol. Mutagen.* **2010**, *51*, 500–507. [[CrossRef](#)]
50. Sarkies, P.; Murat, P.; Phillips, L.G.; Patel, K.J.; Balasubramanian, S.; Sale, J.E. FANCI coordinates two pathways that maintain epigenetic stability at G-quadruplex DNA. *Nucleic Acids Res.* **2012**, *40*, 1485–1498. [[CrossRef](#)]
51. Nelson, J.R.; Lawrence, C.W.; Hinkle, D.C. Deoxycytidyl transferase activity of yeast REV1 protein. *Nature* **1996**, *382*, 729–731. [[CrossRef](#)]
52. Boehm, E.M.; Gildenberg, M.S.; Washington, M.T. The Many Roles of PCNA in Eukaryotic DNA Replication. *Enzymes* **2016**, *39*, 231–254. [[PubMed](#)]
53. Masuda, Y.; Kanao, R.; Kaji, K.; Ohmori, H.; Hanaoka, F.; Masutani, C. Different types of interaction between PCNA and PIP boxes contribute to distinct cellular functions of Y-family DNA polymerases. *Nucleic Acids Res.* **2015**, *43*, 7898–7910. [[CrossRef](#)] [[PubMed](#)]
54. Boehm, E.M.; Powers, K.T.; Kondratick, C.M.; Spies, M.; Houtman, J.C.; Washington, M.T. The Proliferating Cell Nuclear Antigen (PCNA)-interacting Protein (PIP) Motif of DNA Polymerase  $\eta$  Mediates Its Interaction with the C-terminal Domain of Rev1. *J. Biol. Chem.* **2016**, *291*, 8735–8744. [[CrossRef](#)] [[PubMed](#)]
55. Boehm, E.M.; Washington, M.T. R.I.P. to the PIP: PCNA-Binding Motif no Longer Considered Specific: PIP Motifs and other Related Sequences are not Distinct Entities and can Bind Multiple Proteins Involved in Genome Maintenance. *Bioessay* **2016**, *38*, 1117–1122. [[CrossRef](#)]
56. Prestel, A.; Wichmann, N.; Martins, J.M.; Marabini, R.; Kassem, N.; Broendum, S.S.; Otterlei, M.; Nielsen, O.; Willemoes, M.; Ploug, M.; et al. The PCNA interaction motifs revisited: Thinking outside the PIP-box. *Cell Mol. Life Sci.* **2019**, 1–21. [[CrossRef](#)]
57. Petraccone, L.; Spink, C.; Trent, J.O.; Garbett, N.C.; Mekmaysy, C.S.; Giancola, C.; Chaires, J.B. Structure and stability of higher-order human telomeric quadruplexes. *J. Am. Chem. Soc.* **2011**, *133*, 20951–20961. [[CrossRef](#)]
58. Ogloblina, A.M.; Bannikova, V.A.; Khristich, A.N.; Oretskaya, T.S.; Yakubovskaya, M.G.; Dolinnaya, N.G. Parallel G-Quadruplexes Formed by Guanine-Rich Microsatellite Repeats Inhibit Human Topoisomerase, I. *Biochem. (Mosc.)* **2015**, *80*, 1026–1038. [[CrossRef](#)]
59. Azmiri, S.; Lee, J.E. Measuring Protein-Protein and Protein-Nucleic Acid Interactions by Biolayer Interferometry. *Curr. Protoc. Protein Sci.* **2015**, *79*, 19–25.

60. Ciesielski, G.L.; Hytonen, V.P.; Kaguni, L.S. Biolayer Interferometry: A Novel Method to Elucidate Protein-Protein and Protein-DNA Interactions in the Mitochondrial DNA Replisome. *Methods Mol. Biol.* **2016**, *1351*, 223–231.
61. Concepcion, J.; Witte, K.; Wartchow, C.; Choo, S.; Yao, D.; Persson, H.; Wei, J.; Li, P.; Heidecker, B.; Ma, W.; et al. Label-free detection of biomolecular interactions using BioLayer interferometry for kinetic characterization. *Comb. Chem. High Throughput Screen* **2009**, *12*, 791–800. [[CrossRef](#)]
62. Castrec, B.; Rouillon, C.; Henneke, G.; Flament, D.; Querellou, J.; Raffin, J.P. Binding to PCNA in Euryarchaeal DNA Replication requires two PIP motifs for DNA polymerase D and one PIP motif for DNA polymerase B. *J. Mol. Biol.* **2009**, *394*, 209–218. [[CrossRef](#)] [[PubMed](#)]
63. Gulbis, J.M.; Kelman, Z.; Hurwitz, J.; O'Donnell, M.; Kuriyan, J. Structure of the C-terminal region of p21(WAF1/CIP1) complexed with human PCNA. *Cell* **1996**, *87*, 297–306. [[CrossRef](#)]
64. Gueneau, E.; Dherin, C.; Legrand, P.; Tellier-Lebegue, C.; Gilquin, B.; Bonnesoeur, P.; Londino, F.; Quemener, C.; le Du, M.H.; Marquez, J.A.; et al. Structure of the MutLalpha C-terminal domain reveals how Mlh1 contributes to Pms1 endonuclease site. *Nat. Struct Mol. Biol.* **2013**, *20*, 461–468. [[CrossRef](#)] [[PubMed](#)]
65. De March, M.; Merino, N.; Barrera-Vilarmau, S.; Crehuet, R.; Onesti, S.; Blanco, F.J.; de Biasio, A. Structural basis of human PCNA sliding on DNA. *Nat. Commun.* **2017**, *8*, 13935. [[CrossRef](#)] [[PubMed](#)]
66. Pozhidaeva, A.; Pustovalova, Y.; D'Souza, S.; Bezsonova, I.; Walker, G.C.; Korzhnev, D.M. NMR structure and dynamics of the C-terminal domain from human Rev1 and its complex with Rev1 interacting region of DNA polymerase eta. *Biochemistry* **2012**, *51*, 5506–5520. [[CrossRef](#)]
67. Boehm, E.M.; Spies, M.; Washington, M.T. PCNA tool belts and polymerase bridges form during translesion synthesis. *Nucleic Acids Res.* **2016**, *44*, 8250–8260. [[CrossRef](#)]
68. Ohashi, E.; Hanafusa, T.; Kamei, K.; Song, I.; Tomida, J.; Hashimoto, H.; Vaziri, C.; Ohmori, H. Identification of a novel REV1-interacting motif necessary for DNA polymerase kappa function. *Genes Cells* **2009**, *14*, 101–111. [[CrossRef](#)]
69. Hishiki, A.; Hashimoto, H.; Hanafusa, T.; Kamei, K.; Ohashi, E.; Shimizu, T.; Ohmori, H.; Sato, M. Structural basis for novel interactions between human translesion synthesis polymerases and proliferating cell nuclear antigen. *J. Biol. Chem.* **2009**, *284*, 10552–10560. [[CrossRef](#)]
70. Gilljam, K.M.; Feyzi, E.; Aas, P.A.; Sousa, M.M.; Muller, R.; Vagbo, C.B.; Catterall, T.C.; Liabakk, N.B.; Slupphaug, G.; Drablos, F.; et al. Identification of a novel, widespread, and functionally important PCNA-binding motif. *J. Cell Biol.* **2009**, *186*, 645–654. [[CrossRef](#)]



© 2019 by the authors. Licensee MDPI, Basel, Switzerland. This article is an open access article distributed under the terms and conditions of the Creative Commons Attribution (CC BY) license (<http://creativecommons.org/licenses/by/4.0/>).